

Supporting Information

Breaking the Bottleneck of Simultaneously Wide Band Gap and Large Nonlinear Optical Coefficient by “Pore Reconstruction” Strategy in Salt-inclusion Chalcogenide

Shao-Min Pei,^{[a],[b]} Bin-Wen Liu,^[a] * Wen-Fa Chen,^{[a],[b]} Xiao-Ming Jiang,^[a] and Guo-Cong Guo^[a] *

Table of Contents

Experimental Procedures.....	1
Syntheses	1
Structural Refinement and Crystal Data	1
Infrared and UV–Vis–NIR Diffuse Reflectance Spectroscopy.....	1
Second-harmonic Generation Measurement and Laser-induced Damage Thersholt (LIDT) Measurement	1
Thermal Analysis.....	2
Magnetic Measurements.....	2
Computation Procedure	2
Figures and Tables	3
References	9

Experimental Procedures

Syntheses

Single crystal $K_3Rb_3[K_3Cl][Li_2Mn_4Ga_{12}S_{27}]$ (**2**) was prepared by traditional high-temperature solid-state reaction. Approximately 500 mg of unprocessed raw materials with a dosage ratio of La: Mn: Ga: S: LiCl: KCl: RbCl = 1:5:7:17:5:5 were weighed and then cast into the quartz tube. The above operations were performed in an argon-filled glovebox. The quartz tube was sealed under a vacuum of approximately 10^{-4} Torr before being placed in a programmed temperature-controlled muffle furnace. The crude materials were then sintered by the following procedure: heated to 300 °C for 6 h and kept at 300 °C for 6 h, subsequently heated to 600 °C for 6 h and run at 600 °C for 6 h, and then held on 900 °C for 12 h, held at a constant temperature for 96 h, finally cooled down to 300 °C for 96 h before naturally cooling. The clubbed crystals were isolated after the products were washed in deionized water to remove the unreacted cosolvent. Semiquantitative microprobe element analysis of **2** was proceeded by a Hitachi S-3500 SEM spectrometer equipped with energy-dispersive X-ray spectroscopy (EDS). The empirical element molar ratios were K: Rb: Cl: Mn: Ga: S = 4.3: 2.5: 1: 1.8: 10: 25.5, which was in accordance with the experimental formula (Fig. S2).

Structural Refinement and Crystal Data

A Rigaku Pilatus CCD diffractometer outfitted with graphitic monochromatic Mo- $K\alpha$ radiation ($\lambda = 0.71073 \text{ \AA}$) was charged with acquiring single-crystal XRD data sets at 293 K temperature. The primary positions of the atoms were ascertained with the aid of the direct methods, and the coarse structure was refined via the full-matrix least-squares method on F^2 . All operations are fully supported by the Siemens SHELXTL version 5 package of crystallographic software.^{1,2} Data of powder XRD for confirming the purity of **2** was gathered by Rigaku MiniFlex 600 X-ray diffractometer furnished with a diffraction monochromator for Cu- $K\alpha$ radiation ($\lambda = 1.54057 \text{ \AA}$) (Fig. S3).

Infrared and UV–Vis–NIR Diffuse Reflectance Spectroscopy

UV-Vis-NIR diffuse reflectance spectrum of the title compound over the wavelength range of 200–2500 nm was included by a Perkin-Elmer Lambda 900 UV-Vis spectrophotometer, where $BaSO_4$ served as a reference. The absorption spectrum utilized to intercept the band gap was gained by switching the reflection spectrum via the Kubelka-Munk formula: $\alpha/S = (1-R)^2/2R$,³ where α denotes the absorption coefficient, S denotes the scattering coefficient, while R denotes the reflectance. A Nicolet Magana 750 FT-IR spectrophotometer was chosen to generate an IR spectrum of **2** at a wavelength range of 4000–400 cm^{-1} .

Second-harmonic Generation (SHG) and Laser-induced Damage Thersholt (LIDT) Measurement

Finely selected microcrystalline **1**, **2** and commercially acquired AgGaS₂ (AGS) were ground and sifted into five particle sizes covering the ranges of 30–50, 50–75, 75–100, 100–150, and 150–200 μm , respectively, for the purpose of phase-matchable measurements under the guidance of the modified Kurtz-Perry powder method.⁴ The SHG signals in response to 1910 nm laser irradiation were harvested by a charge-coupled device (CCD). The conventional S-on-1 method was suitable for LIDT measurements on polished single crystal slices of **1**, **2** and AGS, where the

adopted laser wavelength is 1064 nm and the pulse width τ_p is 10 ns. Specifically, irradiating the surface with a low-energy laser at first and then gradually increasing the power until damage occurs to the sample. Recording the laser energy (E) precisely, as well as the spot area (πr^2), then the measured LIDT could be calculated by equation $I_{(\text{threshold})} = E/(\pi r^2 \tau_p)$.

Thermal Analysis

A TGA/DSC1 Mettler ToledoS6 thermal analyzer was deployed to investigate differential scanning calorimetry (DSC) analysis of **1** and **2**. Approximately 10 mg of powder samples were packed into a pocket silica tube, evacuated to 10^{-4} Torr, and then flame sealed. The sample-filled and empty tubes were placed on the left and right sides of the analyzer's balance, and then heated from room temperature to 1000°C at 10°C/min and cooled to room temperature at the same rate to accomplish a cycle.

Magnetic Measurements

The magnetic properties of **2** was measured on a Quantum Design PPMS-16 T physical properties tester at an external magnetic field of 1000 Oe in the temperature range of 2–300 K. The magnetic susceptibility measurement exhibits a $\chi_m T$ of 4.237 emu·K·mol⁻¹ at room temperature, which is approximate to the spin-only value of 4.375 emu·K·mol⁻¹ for un-coupled high spin Mn²⁺ ($S = 5/2$, $g = 2$). With the decrease of temperature, the magnetic susceptibility decreases gradually and then sharply, implying that there is an anti-ferromagnetic exchange between Mn²⁺ (Fig. S6).

Computation Procedure

The CASTEP module equipped in the Materials Studio package was employed to study the band structure of **2** based on density functional theory (DFT).⁵⁻⁸ The generalized gradient approximation (GGA) parameterized by Perdew, Burke, and Ernzerhof (PBE) was adopted as the exchange-correlation function. The orbital electrons configurations of Li-1s²2s¹, Rb-4s²4p⁶5s¹, K-3s²3p⁶4s¹, Mn-3p⁶3d⁵4s², Ga-3d¹⁰4s²4p¹, S-3s²3p⁴, and Cl-3s²3p⁵ were selected as valence electrons for further estimating, wherein a plane-wave energy cut-off was 18 Hartree. A $2 \times 2 \times 5$ Monkhorst-Pack κ -point grid was taken for the numerical integration of the Brillouin zone. The linear or nonlinear optical properties of the title compound were evaluated by the ABINIT package based on DFT. An scissors operator of 2.863 eV for compound **2** was applied to move the simulated (0.447 eV) to experimental band gap. The calculated Frequency-dependent SHG susceptibility tensors $\chi_{ijk}(2\omega, \omega, \omega)$ were abided by the density functional perturbation theory and “sum over states” method. And basically, the major contributions of SHG susceptibility can be divided into major kinds usual: the interband transitions, intraband transitions, and modulation of interband terms by intraband terms, which were expressed as $\chi^{\text{inter}}(2\omega, \omega, \omega)$, $\chi^{\text{intra}}(2\omega, \omega, \omega)$, and $\chi^{\text{mod}}(2\omega, \omega, \omega)$, respectively.⁹ The orbital-resolved SHG susceptibility tensors could be worked out via multiplying $\chi^{\text{inter}}(2\omega, \omega, \omega)$, $\chi^{\text{intra}}(2\omega, \omega, \omega)$, and $\chi^{\text{mod}}(2\omega, \omega, \omega)$ by the normalized partial density of the involved orbitals, respectively. And the atom-involved SHG susceptibility tensors were obtained by summing all the orbitals contributions attributed to the target atoms.

Figures and Tables

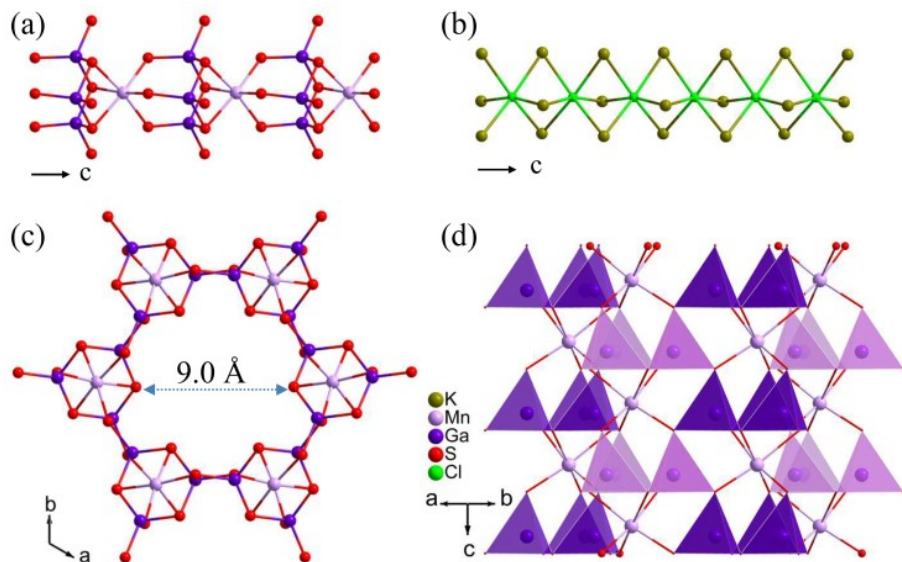


Fig. S1 (a) $[\text{MnGa}_3\text{S}_6]^-$ chain, (b) $[\text{K}_3\text{Cl}]^{2+}$ chain, (c) nano-tunnel built by six $[\text{MnGa}_3\text{S}_6]^-$ units, and (d) $[\text{MnGa}_3\text{S}_6]^-$ anion packing with highly oriented GaS_4 tetrahedra of compound 1.

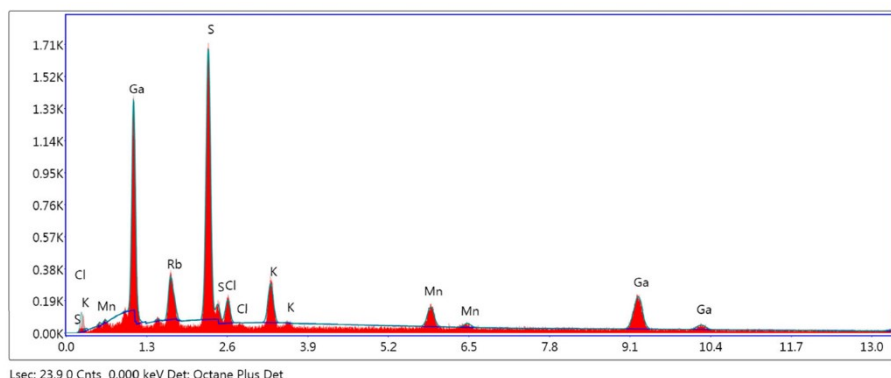


Fig. S2 The EDS results of 2.

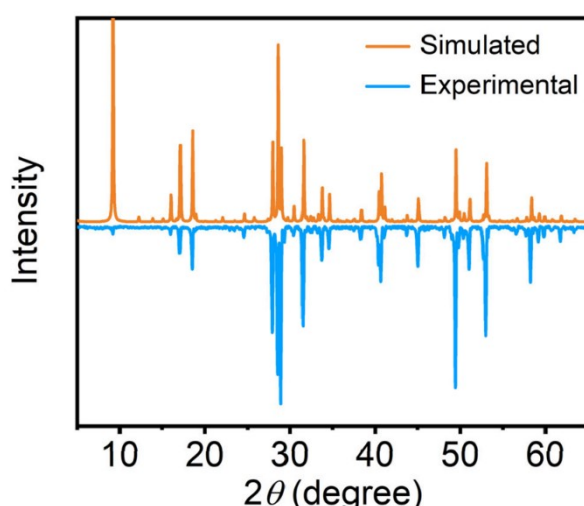


Fig. S3 The experimental and simulated XRD patterns of 2.

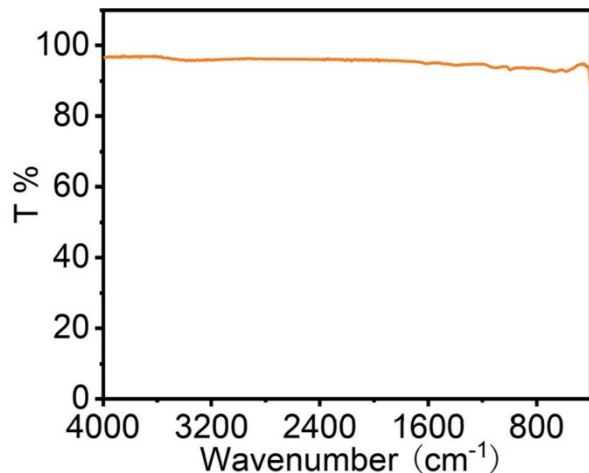


Fig. S4 The IR spectra of **2**.

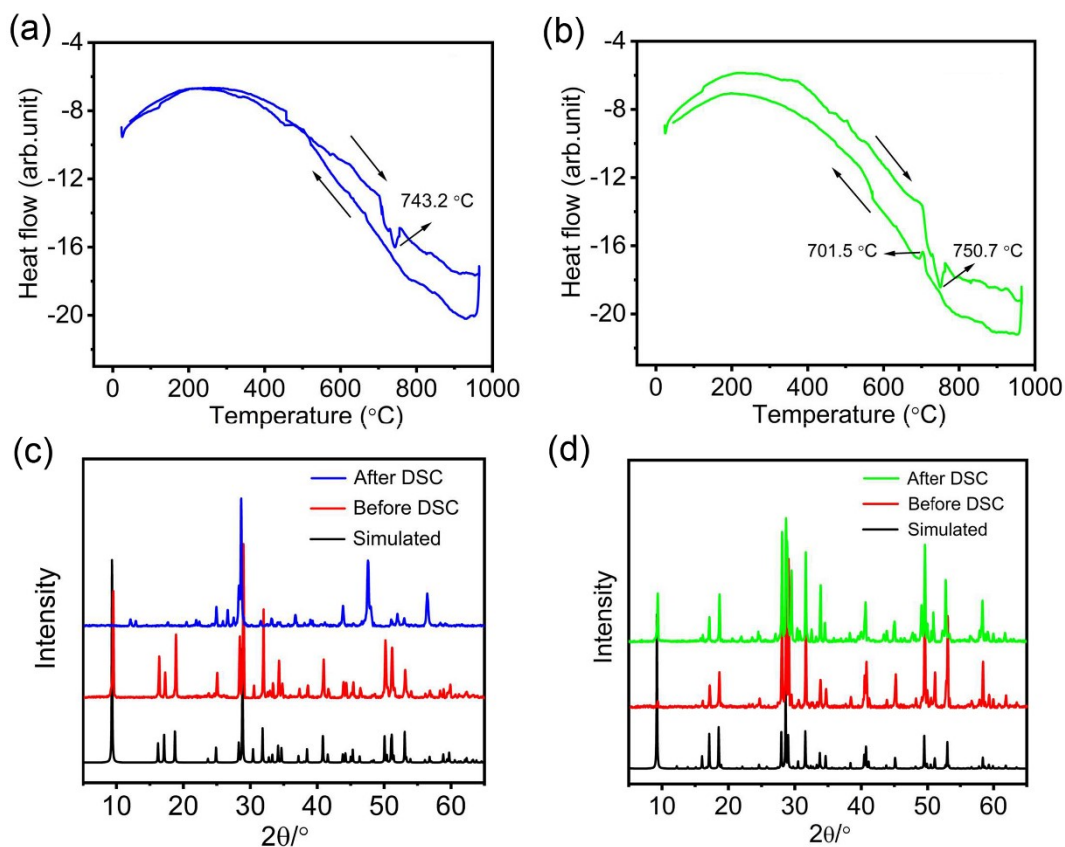


Fig. S5 DSC curves of **1** (a) and **2** (b) upon heating and followed by cooling. Powder XRD patterns of the simulated, before DSC and after DSC measurements for **1** (c) and **2** (d).

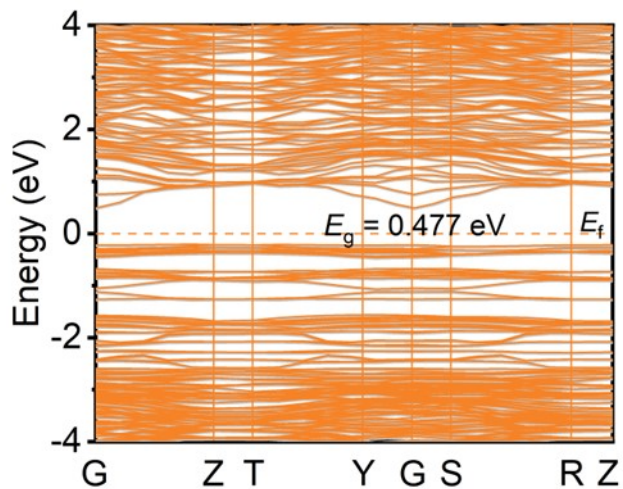


Fig. S6 Band structures of up-spin (green line) and down-spin (violet line) for the antiferromagnetic state of **2**.

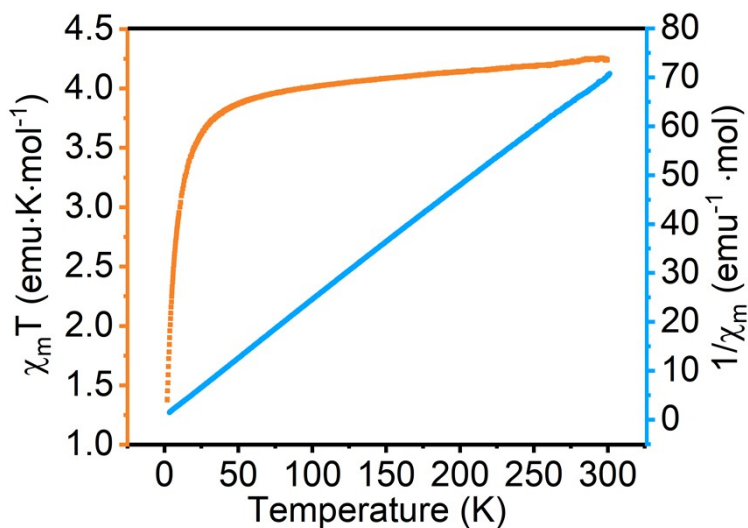


Fig. S7. Variable-temperature $\chi_m T$ and $1/\chi_m$ curves of **2**.

Table S1 Crystallographic data and structure refinement parameters for **2**.

Empirical formula	$K_3Rb_3[K_3Cl][Li_2Mn_4Ga_{12}S_{27}]$ (2)
CCDC	2179230
F_w	2462.36
Temperature (K)	293(2)
Space group	$P6_3mc$
a (Å)	22.0822(4)
c (Å)	6.1544(2)
V (Å ³)	2598.97(13)
Z	2

D_{calcd} (g·cm ⁻³)	3.147
m (mm ⁻¹)	11.460
GOF on F^2	1.064
R_1^a ($I > 2\sigma(I)$)	0.0573
wR_2^b ($I > 2\sigma(I)$)	0.1829
R_1^a (all data)	0.0617
wR_2^b (all data)	0.1883
$\Delta\rho_{\max}/\Delta\rho_{\min}$ (e Å ⁻³)	2.51/-1.61

^a $R = \sum |F_o| - |F_c| | / \sum |F_o|$, ^b $wR = (\sum (w(F_o^2 - F_c^2)^2) / \sum (w(F_o^2)^2))^{1/2}$.

Table S2 Coordinates and equivalent isotropic displacement parameters of all crystallographically independent atoms in **2**.

Atoms	x	y	z	$U^{(\text{eq})}$
K1/Rb1	0.06310(14)	0.44318(15)	0.2346(11)	0.0717(12)
K2	0.0637(2)	0.9363(2)	0.280(3)	0.144(7)
Li1/Mn1	0.6027(3)	0.3973(3)	0.151(2)	0.057(3)
Mn2	0.16631(6)	0.83369(6)	0.0504(8)	0.0180(8)
Ga1	0.27825(4)	0.72175(4)	0.1418(3)	0.0091(5)
Ga2	0.77904(4)	0.22096(4)	0.1409(3)	0.0096(5)
Ga3	0.27524(6)	0.05557(7)	0.13806(18)	0.0093(5)
S1	0.22289(12)	0.77711(12)	0.2744(9)	0.0185(13)
S2	0.39201(10)	0.60799(10)	0.2480(9)	0.0135(11)
S3	0.72370(11)	0.27630(11)	0.2683(8)	0.0109(11)
S4	0.38538(14)	0.11002(13)	0.2787(6)	0.0114(8)
S5	0.05407(19)	0.27645(18)	0.2713(8)	0.0213(12)
S6	0.89080(10)	0.10920(10)	0.2772(7)	0.0129(10)
S7	0.53855(15)	0.46145(15)	0.1988(15)	0.0497(17)
Cl1	0.0000	0.0000	0.000(12)	0.25(2)

Table S3 Selected bond lengths [Å] for **2**.

Bond	Distance	Bond	Distance
K2–Cl1×3	2.79(4)	Ga1–S1	2.269(5)
K2–Cl1×3	2.98(5)	Ga1–S2×2	2.275(3)
Mn2–S5×2	2.541(5)	Ga1–S3	2.300(5)
Mn2–S4×2	2.673(5)	Ga2–S1	2.257(6)
Mn2–S1	2.566(6)	Ga2–S3	2.257(5)
Mn2–S6	2.756(6)	Ga2–S4×2	2.285(3)

Li1/Mn1-S3×2	2.436(8)	Ga3-S5	2.252(4)
Li1/Mn1-S7	2.470(13)	Ga3-S5	2.258(5)
Li1/Mn1-S2	2.488(13)	Ga3-S4	2.277(3)
		Ga3-S6	2.280(3)

Table S4 The laser-induced damage threshold of **1**, **2**, and AgGaS₂ determined by single crystals. (Both **1** and **2** was measured by three times with different single crystals.)

Compounds	Damage energy (mJ)	Spot area (cm ²)	τ_p (ns)	Damage threshold	
				[MW·cm ⁻²]	
1(a)	10.2	0.015	10	66.3	
1(b)	10.7	0.015	10	71.3	
1(c)	9.7	0.015	10	64.6	
2(a)	12.3	0.015	10	82.0	
2(b)	12.0	0.015	10	80.0	
2(c)	12.7	0.015	10	84.6	
AgGaS ₂	1.5	0.015	10	9.7	

Table S5 The average orbital-resolved contributions (%) of each atom type in **2** to the total SHG coefficient tensors (d_{31} and d_{33}) at 1910 nm (0.65 eV) incident laser.

SHG(%)	S-s	S-p	Cl-s	Cl-p	Li-s	K-s	K-p	Rb-s	Rb-p
d_{31}	5.721	62.08	0.036	2.211	0.103	0.014	0.052	0.187	0.194
d_{33}	3.758	62.58	0.006	0.924	0.147	0.066	0.099	0.203	1.119
Average	4.739	62.33	0.021	1.568	0.125	0.040	0.076	0.195	0.656
SHG(%)	Mn-s	Mn-p	Mn-d	Ga-s	Ga-p	Ga-d			
d_{31}	1.139	0.175	5.272	17.35	4.317	1.149			
d_{33}	0.368	0.154	13.26	16.81	0.330	0.176			
Average	0.754	0.164	9.266	17.08	2.324	0.662			

Table S6 Comparison of the major optical parameters of the salt-inclusion chalcogenides reported in the past decade.

Compounds	SHG (xAGS)	Band gap	LIDT (xAGS)
[NaBa ₄ Cl][Ge ₃ S ₁₀] ¹⁰	0.30 (NPM)	3.49	NA
[NaSr ₄ Cl][Ge ₃ S ₁₀] ¹¹	1.08 (NPM)	3.54	11
[KSr ₄ Cl][Ge ₃ S ₁₀] ¹¹	0.91 (NPM)	3.51	12
[KBa ₄ Cl][Ge ₃ S ₁₀] ¹¹	0.82 (NPM)	3.57	12
[Ba ₄ Cl ₂][Ge ₃ S ₉] ¹²	2.40 (NPM)	2.91	NA
[Ba ₄ Cl ₂][Ge ₃ Se ₉] ¹²	0.50 (NPM)	1.76	NA
[Ba ₄ Cl ₂][Si ₃ Se ₉] ¹²	0.50 (NPM)	1.89	NA

[Ba ₄ Br ₂][Si ₃ Se ₉] ¹³	3.20 (NPM)	2.96	NA
[Ba ₄ Br ₂][Ge ₃ Se ₉] ¹³	3.50 (NPM)	2.60	NA
[K ₂ Ba ₃ Cl ₂][Ge ₃ S ₉] ¹⁴	0.34 (NPM)	3.69	28.8
[Sr ₄ Cl ₂][Si ₃ S ₉] ¹⁵	1.2	4.22	12
[K ₃ Cl][Ga ₃ PS ₈] ¹⁶	1.00	3.60	39
[Rb ₃ Cl][Ga ₃ PS ₈] ¹⁶	1.10	3.65	37
[K ₃ Br][Ga ₃ PS ₈] ¹⁶	1.20	3.85	32
[Rb ₃ Br][Ga ₃ PS ₈] ¹⁶	2.00	3.50	31
[RbBa ₂ Cl][Ga ₄ S ₈] ¹⁷	1.00	3.30	11
[CsBa ₂ Cl][Ga ₄ S ₈] ¹⁷	0.90	3.35	12
Li[LiCs ₂ Cl][Ga ₃ S ₆] ¹⁸	0.70	4.18	4.1 (Single crystal)
[Ba ₃ KCl ₂][Ga ₅ Se ₁₀] ¹⁹	10 (NPM)	3.22	NA
[Ba ₃ RbCl ₂][Ga ₅ Se ₁₀] ¹⁹	20 (NPM)	3.23	NA
[Ba ₃ CsCl ₂][Ga ₅ Se ₁₀] ¹⁹	100 (NPM)	3.25	NA
[Ba ₄ Cl ₂][ZnGa ₄ Se ₁₀] ²⁰	59 (NPM)	3.08	17
[Ba ₄ Cl ₂][CdGa ₄ Se ₁₀] ²⁰	52 (NPM)	2.93	NA
[Ba ₄ Cl ₂][MnGa ₄ Se ₁₀] ²⁰	30 (NPM)	2.78	NA
[Ba ₄ Cl ₂][CuGa ₄ Se ₁₀] ²⁰	39 (NPM)	2.54	NA
[Ba ₄ Cl ₂][CoGa ₄ Se ₁₀] ²⁰	NA	2.25	NA
[Ba ₄ Cl ₂][FeGa ₄ Se ₁₀] ²⁰	NA	1.88	NA
[CsBa ₃ Cl ₂][In _{0.5} Ga _{4.5} Se ₁₀] ²¹	64 (NPM)	3.01	16.5
[CsBa ₃ Cl ₂][InGa ₄ Se ₁₀] ²¹	70 (NPM)	2.90	16.2
[Ba ₄ Cl ₂][ZnGa ₄ S ₁₀] ²²	1.1	3.85	51
[Ba ₄ Cl ₂][HgGa ₄ S ₁₀] ²³	1.5	2.95	15
[KBa ₃ Cl ₂][Ga ₅ S ₁₀] ²⁴	1.0	3.93	6.7 (Single crystal)
[RbBa ₃ Cl ₂][Ga ₅ S ₁₀] ²⁴	1.0	3.95	6.5 (Single crystal)
[CsBa ₃ Cl ₂][Ga ₅ S ₁₀] ²⁴	1.0	3.96	6.3 (Single crystal)
[K ₄ Cl][CdGa ₉ S ₁₆] ²⁵	0.90	3.14	22.6
[K ₄ Cl][CdGa ₉ Se ₁₆] ²⁵	2.40	1.72	7.7
[Rb ₄ Cl][Cd ₁₁ In ₉ S ₂₆] ²⁶	0.23	2.32	4.9
[K ₂ PbCl][Ga ₇ S ₁₂] ²⁷	2.5	2.54	2.5
[K ₂ PbBr][Ga ₇ S ₁₂] ²⁷	2.6	2.49	2.3
[K ₂ PbI][Ga ₇ S ₁₂] ²⁷	2.7	2.41	4.0
(K ₃ I)[InB ₁₂ (InSe ₄) ₃] ²⁸	0.07×KTP	1.97	NA
(K ₃ Cl)[InB ₁₂ (InS ₄) ₃] ²⁹	0.18 (Cal.)	1.76 (Ca.)	NA
(K ₃ Br)[InB ₁₂ (InS ₄) ₃] ²⁹	0.18 (Cal.)	1.77 (Ca.)	NA
(K ₃ I)[InB ₁₂ (InS ₄) ₃] ²⁹	0.18 (Cal.)	1.83 (Ca.)	NA

(Cs ₃ I)[InB ₁₂ (InS ₄) ₃] ²⁹	0.20 (Cal.)	1.83 (Ca.)	NA
(K ₃ I)[GaB ₁₂ (GaS ₄) ₃] ²⁹	0.18 (Cal.)	1.95 (Ca.)	NA
(K ₃ I)[GdB ₁₂ (GaS ₄) ₃] ²⁹	0.19 (Cal.)	2.05 (Ca.)	NA
(K ₃ I)[SmB ₁₂ (GaS ₄) ₃] ³⁰	0.30×KDP	2.35	NA
(Rb ₃ I)[InB ₁₂ (InS ₄) ₃] ³⁰	0.15 (Cal.)	1.94 (Ca.)	NA
(K ₃ Cl)[InB ₁₂ (InSe ₄) ₃] ³⁰	0.30×KDP	2.02	NA
(K ₃ Br)[InB ₁₂ (InSe ₄) ₃] ³⁰	0.20	1.54 (Ca.)	NA
(Rb ₃ I)[InB ₁₂ (InSe ₄) ₃] ³⁰	0.20	1.55 (Ca.)	NA
(Cs ₃ Cl)[InB ₁₂ (InSe ₄) ₃] ³⁰	0.20	1.59 (Ca.)	NA
(Cs ₃ I)[InB ₁₂ (InSe ₄) ₃] ³⁰	0.20	1.57 (Ca.)	NA
[K ₃ Cl][Mn ₂ Ga ₆ S ₁₂] ³¹	0.8	3.17	6.9 (Single crystal)
K ₃ Rb ₃ [K ₃ Cl][Li ₂ Mn ₄ Ga ₁₂ S ₂₇] (this work)	1.1	3.31	8.5 (Single crystal)

NA = Not Available.

References

1. G. M. Sheldrick, University of Gö ttingen: Gö ttingen, Germany, 1997.
2. Rigaku Oxford Diffraction, CrysAlisPro Software System, Version v40.67a, Rigaku Corporation, Oxford, UK, 2019.
3. G. Korum., Springer: New York, 1969.
4. S. K. Kurtz. and T. T. Perry., *J. Appl. Phys.*, 1968, **39**, 3798–3813.
5. S. Baroni, S. Gironcoli, A. D. Corso. and P. Giannozzi., *Rev. Mod. Phys.* , 2001, 515–562.
6. P. Ghosez, X. Gonze. and R. W. Godby., *Phys. Rev. B*, 1997, **56**, 12811–12817.
7. X. Gonze., *Phys. Rev. A*, 1995, **52**, 1096–1114.
8. X. Gonze., *Phys. Rev. A*, 1995, **52**, 1086–1095.
9. S. Sharma. and C. A. Draxl., *Phys. Scr.* , 2004, **T109**, 128–134.
10. K. Feng, L. Kang, Z. S. Lin, J. Y. Yao and Y. C. Wu, *J. Mater. Chem. C*, 2014, **2**, 4590-4596.
11. Y. Song, S. Cui, Z. Qian, H. Yu, Z. Hu, J. Wang, Y. Wu and H. Wu, *Inorg. Chem. Front.*, 2022, **9**, 5932-5940.
12. P. F. Liu, Y. Y. Li, Y. J. Zheng, J. S. Yu, R. H. Duan, H. Chen, H. Lin, L. Chen and L. M. Wu, *Dalton Trans.*, 2017, **46**, 2715-2721.
13. W. Xing, N. Wang, A. K. Iyer, W. Yin, Z. Lin, J. Yao, B. Kang and A. Mar, *J. Alloys Compd.*, 2020, **846**.
14. W. Zhou, Z.-H. Shi, W. Liu and S.-P. Guo, *J. Alloys Compd.*, 2022, **895**.
15. C. Zhao, K. Wu, Y. Xiao, B. Zhang, H. Yu and H. Zhang, *J. Mater. Chem. C*, 2023, **11**, 4439-4443.
16. B. W. Liu, H. Y. Zeng, X. M. Jiang, G. E. Wang, S. F. Li, L. Xu and G. C. Guo, *Chem. Sci.* , 2016, **7**, 6273-6277.
17. B.-W. Liu, X.-M. Jiang, H.-Y. Zeng and G.-C. Guo, *J. Am. Chem. Soc.*, 2020, **142**, 10641-10645.
18. B.-W. Liu, X.-M. Jiang, B.-X. Li, H.-Y. Zeng and G.-C. Guo, *Angew. Chem. Int. Ed.*, 2020, **59**, 4856-4859.
19. P. Yu, L. J. Zhou and L. Chen, *J. Am. Chem. Soc.*, 2012, **134**, 2227-2235.
20. Y. Y. Li, P. F. Liu, L. Hu, L. Chen, H. Lin, L. J. Zhou and L. M. Wu, *Adv. Optical Mater.*, 2015, **3**, 957-966.
21. Y. Y. Li, P. F. Liu, H. Lin, M. T. Wang and L. Chen, *Inorg. Chem. Front.*, 2016, **3**, 952-958.
22. H. Chen, Y.-Y. Li, B. Li, P.-F. Liu, H. Lin, Q.-L. Zhu and X.-T. Wu, *Chem. Mater.*, 2020, **32**, 8012-8019.
23. Y. Zhang, H. Wu, Z. Hu, J. Wang, Y. Wu and H. Yu, *Inorg. Chem. Front.*, 2022, **9**, 4075-4080.
24. B.-W. Liu, H.-Y. Zeng, X.-M. Jiang and G.-C. Guo, *CCS Chem.*, 2021, **3**, 964-973.
25. S.-M. Pei, B.-W. Liu, X.-M. Jiang, Y.-Q. Zou, W.-F. Chen, Q.-N. Yan and G.-C. Guo, *Chem. Mater.*, 2021, **33**, 8831-8837.
26. S.-M. Pei, L.-T. Jiang, B.-W. Liu and G.-C. Guo, *J. Alloys Compd.*, 2022, **902**.
27. W. F. Chen, B. W. Liu, S. M. Pei, X. M. Jiang and G. C. Guo, *Adv. Sci.* , 2023, e2207630.
28. S. P. Guo, Y. Chi, B. W. Liu and G. C. Guo, *Dalton Trans.*, 2016, **45**, 10459-10465.
29. Z.-D. Sun, Y. Chi, H.-G. Xue and S.-P. Guo, *Inorg. Chem. Front.*, 2017, **4**, 1841-1847.
30. S.-S. Han, W.-D. Yao, S.-X. Yu, Y. Sun, A. Gong and S.-P. Guo, *Inorg. Chem.*, 2021, **60**, 3375-3383.

